Asian Journal of Geological Research

Volume 7, Issue 2, Page 136-153, 2024; Article no.AJOGER.119595

Integrated Interpretation of Aeromagnetic and Aero-radiometric Data to Delineate Structures and Hydrothermal Alteration Zones Associated with Gold Mineralization in Parts of North-Central Nigeria

Bwamba, Jonah Ayuba [a*] and Abu Mallam [a]

[a] *Physics Department, University of Abuja, Abuja, Nigeria.*

Authors' contributions

This work was carried out in collaboration between both authors. Both authors read and approved the final manuscript.

Article Information

Open Peer Review History:
This journal follows the Advanced Open Peer Review policy. Identity of the Reviewers, Editor(s) and additional Reviewers, peer review comments, different versions of the manuscript, comments of the editors, etc are available here: https://www.sdiarticle5.com/review-history/119595

Original Research Article

Received: 29/05/2024
Accepted: 01/07/2024
Published: 05/07/2024

ABSTRACT

Locating zones of possible gold mineralization potentials in parts of north-central Nigeria has been performed in this work by mapping lithology, structures, and hydrothermal alteration regions from aeromagnetic and aeroradiometric data. Some enhancement techniques such as first vertical derivative tilt derivative, analytic signal, and center for exploration targeting grid analysis were used for data analysis and interpretation. The CET grid analysis) reveals that the extracted lineaments

**Corresponding author: Email: ynankikwali@yahoo.com;*

Cite as: *Ayuba, Bwamba, Jonah, and Abu Mallam. 2024. "Integrated Interpretation of Aeromagnetic and Aero-Radiometric Data to Delineate Structures and Hydrothermal Alteration Zones Associated With Gold Mineralization in Parts of North-Central Nigeria". Asian Journal of Geological Research 7 (2):136-53. https://journalajoger.com/index.php/AJOGER/article/view/161.*

are primarily oriented in the NE-SW, NNE-SWW and E-W directions. Two to three distinct magnetic zones; the very high, the moderate, and the low magnetic zonesare seen on the analytical signal map. While the high magnetic anomalies correlate with sandstone, siltstone, and shale, the zones of high magnetic anomalies in the northern half are associated to migmatite, gneisses, and biotite. The Euler deconvolution analysis indicates a broad range of depths for the magnetic sources in the region. The sources that are deeper than 2000 meters, between 1000 and 2000 meters, between 500 and 1000 meters, and shallower than 500 meters are specifically indicated by the depth estimates. Furthermore, potential mineralization zones were identified by demarcating areas with hydrothermal alteration zones that align with lineaments obtained from the first vertical derivative map of the studied region. The ternary image showed that coarse porphyritic biotite hornblende granite was primarily linked to the hydrothermally altered zones or mineralized environments in the research area.

Keywords: Gold; mineralization; basement; hydrothermal; alteration.

1. INTRODUCTION

Magnetic surveying explores the subsurface by analysing changes in the Earth's magnetic field caused by the magnetic properties of the underlying rocks. The method of measuring the fluctuation of various important physical or geochemical characteristics of the Earth from the air is known as airborne geophysical surveying.

In engineering applications, hydrocarbon exploration, geothermal operations, mineralization area investigation, and archeological site studies, aeromagnetic and aeroradiometric data have typically shown to be beneficial [1,2,3,4,5,6,7].

Orogenic gold deposits are an important source of the world's gold production. These deposits form along convergent plate boundaries, where compressional or transpressional tectonic forces are at play. During these deformation processes, the gold deposits become localized in metamorphosed rock bands near major crustal-scale fault zones [8]. Robust structural constraints, which are usually found in second or third-order structures, are essential in controlling mineralization. These structures act as conduits for hydrothermal fluids, which have significance for localizing mineralization. To evaluate such deposits, geophysical measurements are essential [9].

Aero-radiometric and high-resolution magnetic mapping, in particular, are commonly used to map concealed geological features that are directly associated to mineralization. These methods are widely employed globally as the main tools for geological interpretations due to their significance in defining geological features such as folds, faults, shear zones, and other mineralization-attractive locations [10,11,12]. The magnetic data has to be enhanced in various ways before any interpretation is possible. The horizontal gradient, tilt angle derivatives, tilt wavelet transforms of horizontal derivatives in possible field data, tilt angle derivatives, and CET grid analysis—an automated technique for identifying lineaments from field data may all be included in these improvements. In orogenic gold deposits, geologic structures have been found using aeromagnetic data [13,14].

Conversely, gamma-ray spectrometry focuses on the distribution of radioelements (K, Th, and U) on the surface of the Earth. Given that different types of rocks have variable quantities of these radioelements, gamma-ray spectrometry can be used to map and categorize distinguished lithological units. [15,16,17,18,19]. Many authors have mapped lithological units using this technique [20,21,22,23, 24,25,26].

Moreover, the identification of hydrothermal alteration zones is a highly accurate and successful application of this methodology. The eTh/K ratio is the best indicator for identifying potassic alteration zones, according to Bwamba et al. [5]. It can also be utilized to infer certain structures that could be undetected ordinarily.

Therefore, as shown by authors in [27,28,29,30,31,5] aero-magnetic and aero-radiometric data can be used to evaluate structural attributes and locate hydrothermal alteration zones.

On the basis of the interpretation of aeromagnetic data, a number works have been published in different sections of the central Nigerian Basement, which presents a complex mineralogical and structural framework with depth to the magnetic source [32,33,34,30]. Their research revealed a number of geological units, including as contact zones and hydrothermal alteration zones that may mineralize into gold deposits

2. LOCATION AND GEOLOGY OF THE STUDY AREA

The research location, which has an estimated area of 18000 Km^2, encompasses longitudes 6° 30' to 7° 30'E and latitudes 8° 00' to 9° 30'N (Fig. 1). The study area is located majorly the on Nigeria's north central region Precambrian Basement (Fig. 2). The Precambrian-aged, high-grade metamorphic and igneous rocks that make up the surface geology primarily trend northeastern to southwest. These rocks are made up of granites, migmatites, and gneiss. There are outcrops of the schist belt along the area's eastern boundary (Fig. 3).

According to Rahaman [35], the rocks fall into the following main categories: Minor intrusions like rhyolites, quartz-feldspar porphyry, dolerites, and basalts; metamorphosed supracrustal rocks (mica schist, marble, amphibolites and amphibole schist, fine-medium grained gneiss); and the Migmatite Complex (migmatite, migmatite gneiss, granite gneiss, porphyroblastic granite gneiss, leucocratic granite gneiss), (Fig. 3). Other materials include quartzite, pegmatite, and quartz vein.

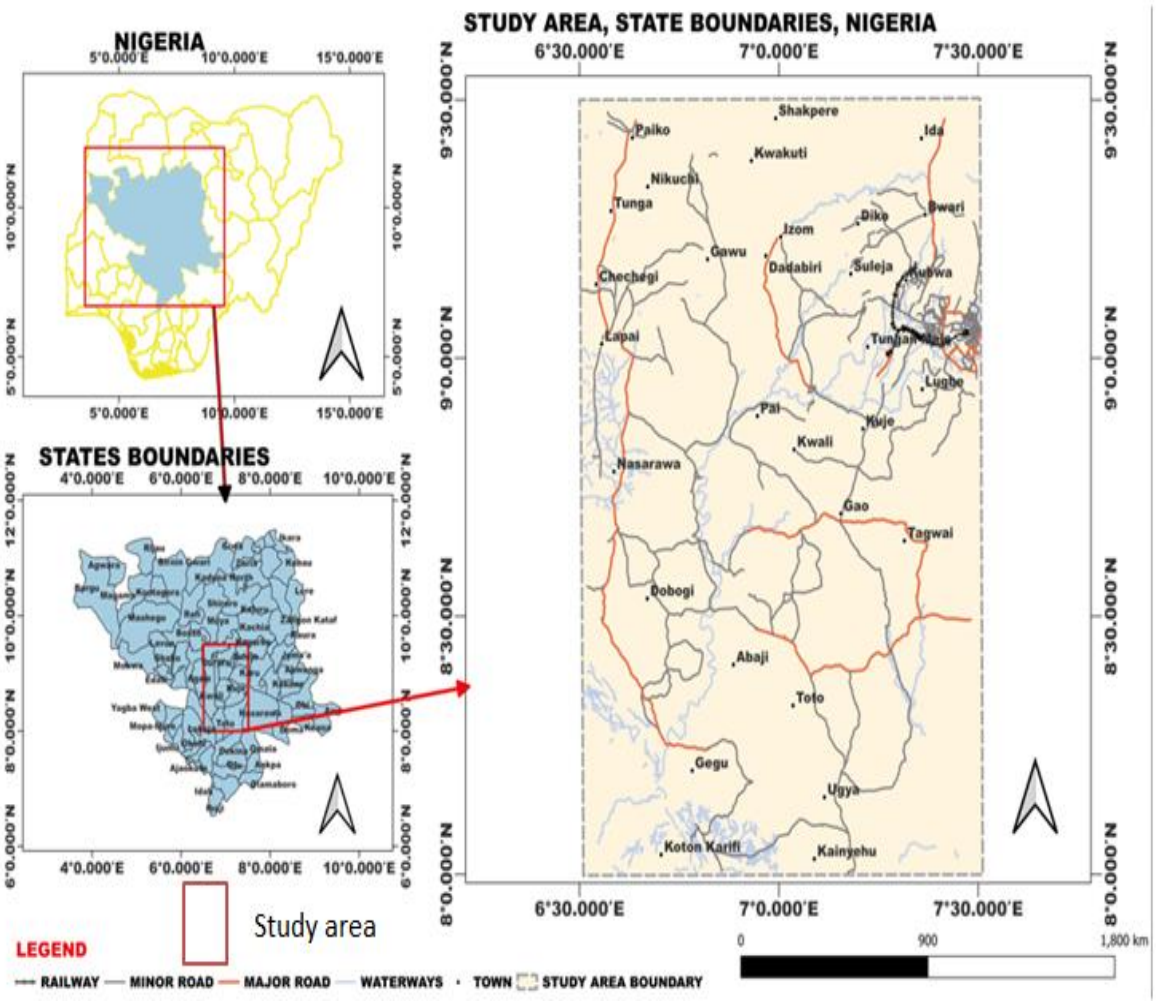

Fig. 1. Location map of the study area

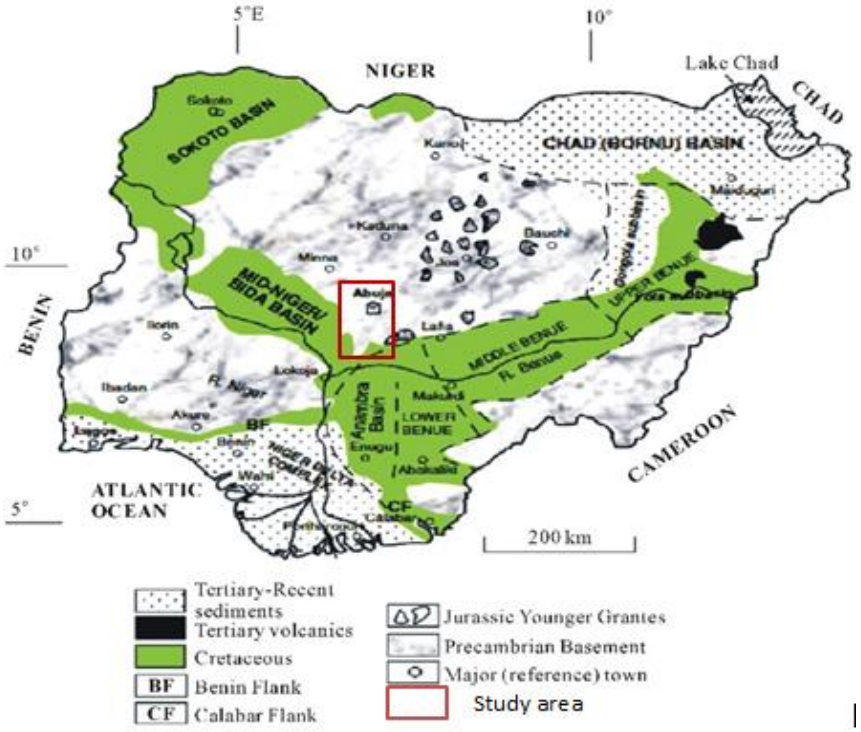

Fig. 2. Geological map of Nigeria showing the study area and major geological components (modified after Obaje [36])

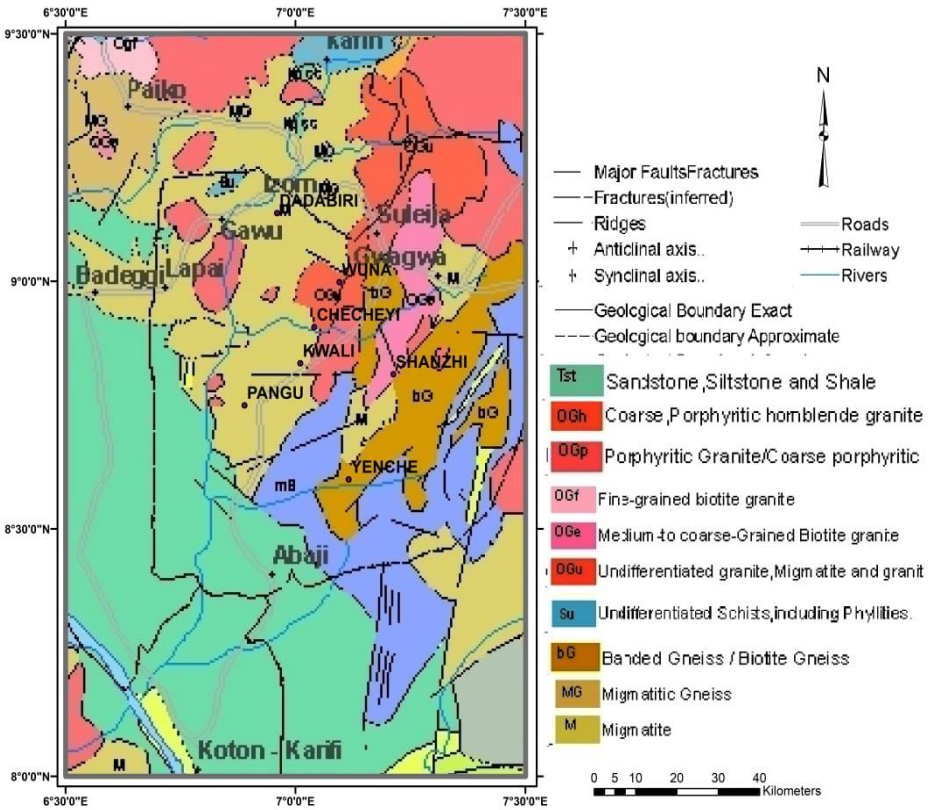

Fig. 3. Geology map of the study area

3. MATERIALS AND METHODS

3.1 Data Source and Acquisition

The Nigeria Geological Survey Agency (NGSA) provided the study with high-quality aerial radiometric data across Nigeria in 2008. The Nigerian government hired the Canadian company Fugro Airborne Surveys Limited to complete the acquisition, primarily for the aim of supplying geological and geophysical data. It was collected during a flight at an altitude of 80 meters, with tie lines spaced 2000 meters apart and lines spaced 500 meters apart. The research region, which is approximately 18,000 Km^2, was formed by knitting six half-degree aeromagnetic and aeroradiometric data sheets, 185 (Paiko), 186 (Abuja), 206 (Gulu), 207 (Kuje), 227 (Koton Karfe), and 228 (Katakwa). The nationwide geophysical survey was concluded in 2010.

3.2 Data Processing and Analysis

To preserve a consistent coordinate system and prevent data misinterpretation, the data obtained from NGSA was produced using Microsoft Excel and processed using Oasis Montaj 8.4v. The data was then imported and converted to UTM zone 32 N.

3.2.1 Aeromagnetic data

Using the International Geomagnetic Reference Field (IGRF 2010), regional abnormalities were removed from the aeromagnetic data through processing. We reduced the overall magnetic intensity map to the equator (Fig. 4) to locate magnetic anomalies above their source bodies and remove the anomalies' tilt. The generated RTE map was then subjected to a number of improvement and filtering processes, which improved the interpretability of the data.

In this work, we specifically used the tilt angle derivative improvements, the analyticl signal and the first vertical derivatives filters to furnished additional insights and revealed specific structural traits crucial for interpretation purposes. The data processing was conducted using Oasis Montaj Geosoft software [37].

a. First vertical derivative

In order to identify the shallowest geological source, the vertical derivative, which can be computed in the frequency or space domain, is frequently applied to total magnetic field data. A cause structure can be imaged more clearly thanks to the enhancement, which tends to reduce anomaly complexity and sharpen anomalies over bodies. Due to its tendency to magnify short wavelength noise, the transition may be loud. In magnetic interpretation projects, first vertical derivative data are now practically essential. Resolving power of the second vertical derivatives is higher than that of the first vertical derivatives [38]. Equation (1) presents the general derivative's algorithm.

$$L(r) = r^n \tag{1}$$

Where n= order of differentiation

b. Analytic signal

The analytic signal filter is applied to identify magnetic discontinuities and expose the boundaries of anomalies. This filter is used on magnetic data with the intention of simplifying the fact that magnetic bodies typically have a positive and negative peak connected with them, which often makes pinpointing the precise location of the causal body challenging. Nabighian [39] has demonstrated that a bell-shaped symmetrical function that maximizes precisely over the top of the magnetic contact may be derived for two-dimensional substances. According to Nabighian [39], the formula for the analytic signal is presented in equation (2):

$$|A(x,y,z)| = \left[\left(\frac{dT}{dx}\right)^2 + \left(\frac{dT}{dy}\right)^2 + \left(\frac{dT}{dz}\right)^2\right]^{\frac{1}{2}} \tag{2}$$

where $|A(x,y,z)|$ is the amplitude of the analytic signal at (x, y, z).

T is the observed magnetic field at (x, y, z).

c. Tilt derivative filter

Tilt derivatives are utilized as an enhancement method for identifying various geological features such as lineaments, faults, joints, contacts, and magnetic source boundaries. Mathematically, the tilt angle (θ) of a magnetic anomaly (A) is equivalent to the local phase presented in equation (3)

$$\theta = \tan^{-1}\left(\frac{\partial A/\partial z}{\partial A/\partial h}\right) \tag{3}$$

where the numerator and denominator are vertical and horizontal derivatives of the anomaly, respectively, the latter given by Verduzo et al. [40], presented in equation (4)

$$\partial A/\partial h = \sqrt{(\partial A/\partial x)^2} + \sqrt{(\partial A/\partial y)^2} \quad (4)$$

The use of the tilt derivative offers several advantages in the interpretation of magnetic anomalies.

d. Euler deconvolution

To estimate source depth of magnetic sources, researchers have used the 3-D Euler deconvolution technique [41]. The method relies on the assumption that anomalous magnetic fields of localized structures are homogeneous functions of the source coordinates and, consequently, satisfy Euler's homogeneity equation. Typically, the structural index (SI) remains fixed, and the locations and depths (x_0, y_0, z_0) of any sources are determined using the following equation (5),

$$\frac{\partial f}{\partial x}(x - x_0) + \frac{\partial f}{\partial y}(y - y_0) + \frac{\partial f}{\partial z}(z - z_o) = SI(B - f) \quad (5)$$

where f is the observed field of location $(x, y \text{ and } z)$ and *f* is the base level of the field [regional value at the point (*x,y,z*)] and *SI* is the structural index or degree of homogeneity.

f. Centre for exploration targeting grid (CET) analysis

According to [37], the CET Grid Analysis is an Oasis montajTM add-on that is intended for exploration targeting. Algorithms in CET automatically detect promising mineral deposit regions and draw boundaries between them. With the use of various statistical techniques like texture analysis, lineation delineation, vectorization, and structural complexity analysis, users of the CET Grid Analysis extension can examine textures, phases, and structures in gridded data. This extension was utilized in our study for threshold identification, edge recognition, grid texture analysis, lineament detection, and heat map generation.

3.2.2 Aero-radiometric data

The aero-radiometric data were processed to create maps visualizing the surface distributions of potassium, equivalent thorium, and equivalent uranium. This aero-radiometric technique has been shown to be highly valuable for identifying areas of hydrothermal alteration and mapping geological units. The Potassium (K), equivalent thorium (eTh ppm), equivalent uranium (eU), and ternary imageries were used in the enhancement processes. These operations resulted in maps that correlate with the pattern and trend of geological units [42]. The ternary map, sometimes referred to as the composite image, was created by estimating the K/eTh ratio and designating the colors red, green, and blue to K, eTh, and eU, respectively. The mapping of hydrothermal alterations and lithological formations was done using the K/eTh ratio and these composite maps, respectively [5].

4. RESULTS AND DICUSSION

4.1 Aeromagnetic Data Interpretation

The research area is characterized by a wide range of values, as shown by the Reduced to the Equator (RTE) map (Fig. 4). Depending on their amplitudes, these values can be divided into different colorations.

Low magnetic anomalies, indicated by blue colour shades ranging from -101 to -14.19 nT, are seen in the research area's southwest corner, the extreme southeast corner, the area around Abaji, Suleja, Zuba and south of Gwarinpa as well as in the northeastern corner of the study area. They are connected to loose sediments. Intermediate-scale colours, ranging from -1.02 to 33.16 nT, are denoted by light green colour shades. These colours mostly cover the areas that are located in the southern part of Gwarinpa, western part of Abaji, the area located far east of Yenche and the areas around Kwali, Dadabiri and north of Zuba. Schists are likely connected to these locations. High amplitude anomalies, indicated by magenta colour shades falling between 38.17 and 101.69 nT and trending in a NW-SE direction which can be mostly seen around Yenche, Pangu, Kwali, Checheyi, Shanzhi, Dadabiri and Abaji in the southern part of the research area. They have similarities with granitic gneiss and biotite lithologic appearance.

Figs. 5 and 6 show the results of the First Vertical and Tilt Derivative filtering application.

In contrast to the southwestern and northeastern regions, the data processing shows that the northwestern and southeastern parts of the research area exhibit short-wavelength anomalies, indicating shallower depths of causal sources. These areas are thought to be large fractures or faults and are characterized by formations that primarily follow a northwest-southeast trend.

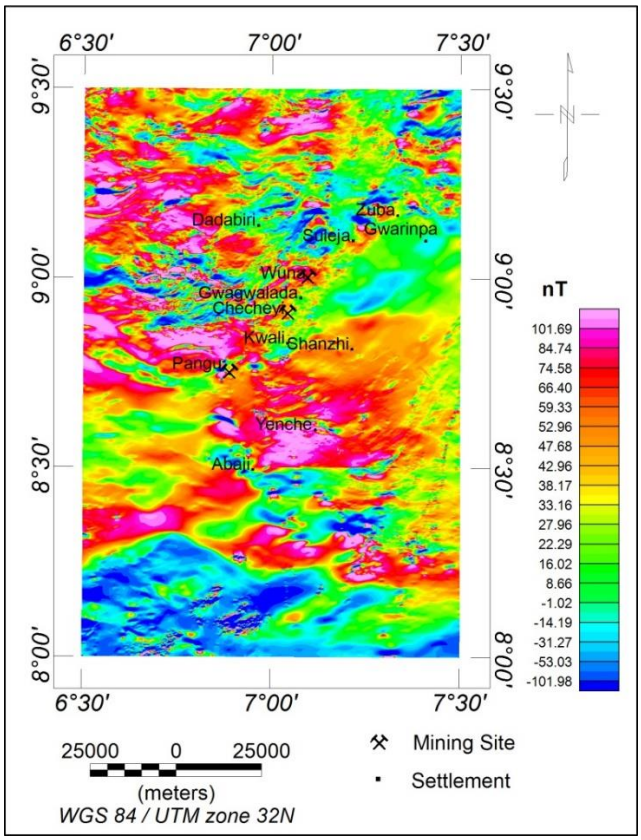

Fig. 4. Reduced to the Equator map (RTE) of the study area

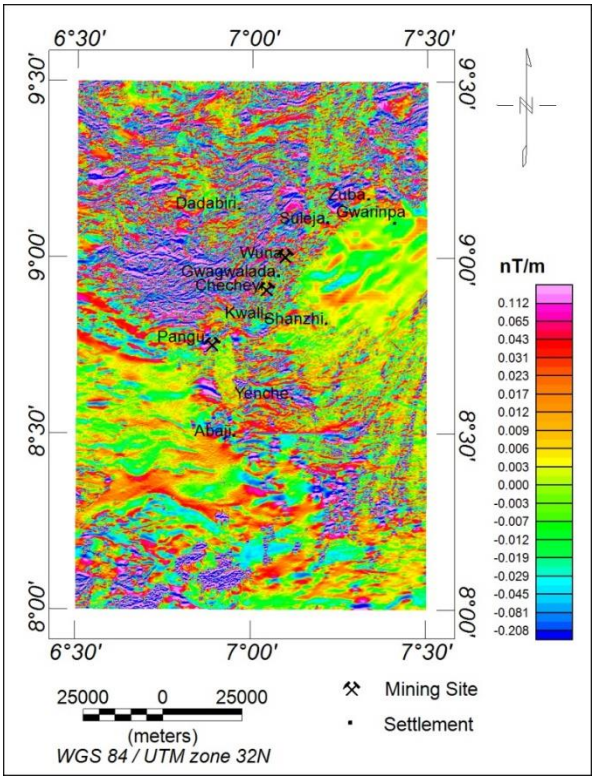

Fig. 5. First Vertical Derivative map of the study area

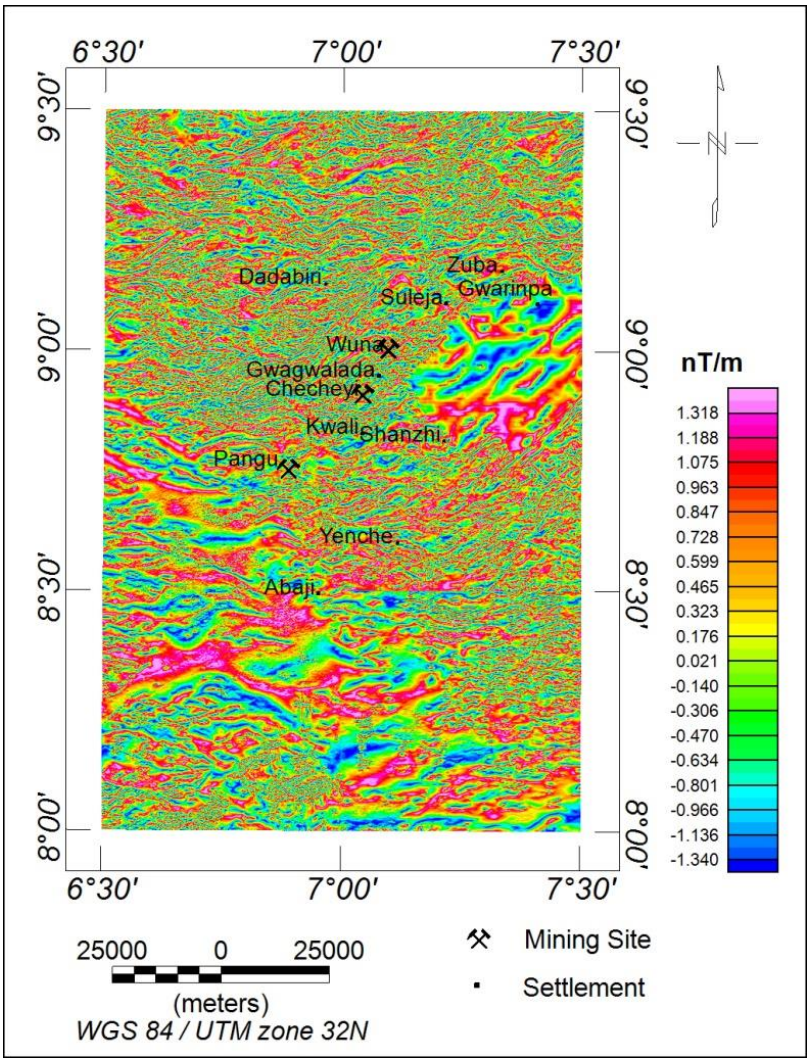

Fig. 6. Tilt Derivative map of the study area

The RTE map was subjected to CET grid analysis using the procedures described in section 3.2.1e above to find linear structures. Figs. 7a and 7b show the distribution of lineaments extracted using CET. The Rose diagram (Fig. 7b) reveals that the extracted lineaments are primarily oriented in the NE-SW, NNE-SWW and E-W directions. Given the faulting in the region, the long linear features are believed to be large fractures or faults. These structural features, such as faults, shear zones, and fractures, may have served as conduits for magmatic or hydrothermal processes. This could have led to deposition of minerals within the affected areas. This pattern suggests that the deep, underlying rock layers in the Earth's crust have significant variations in their composition and structure. These heterogeneities in the deep crust are influencing the overlying basement rock complex through the presence of fractures and faults that allow interactions between the different rock layers. In other words, the variations and discontinuities within the deeper crustal rocks are being expressed and manifested in the shallower basement complex through the network of cracks and fault zones that connect them. . Furthermore, upon examining the map (Fig. 7a), it becomes evident that the northern portions of the area's basement rocks have experienced significant deformation. These findings offer crucial insights into the basement-level fractures and faults that have impacted this geographical area. There appear to be structural control on the area's potential for mineralization as the predominant concentration of the lineaments correspond with the mining sites of Checheyi, Pangu and Wuna all located within the northern half of the study area.

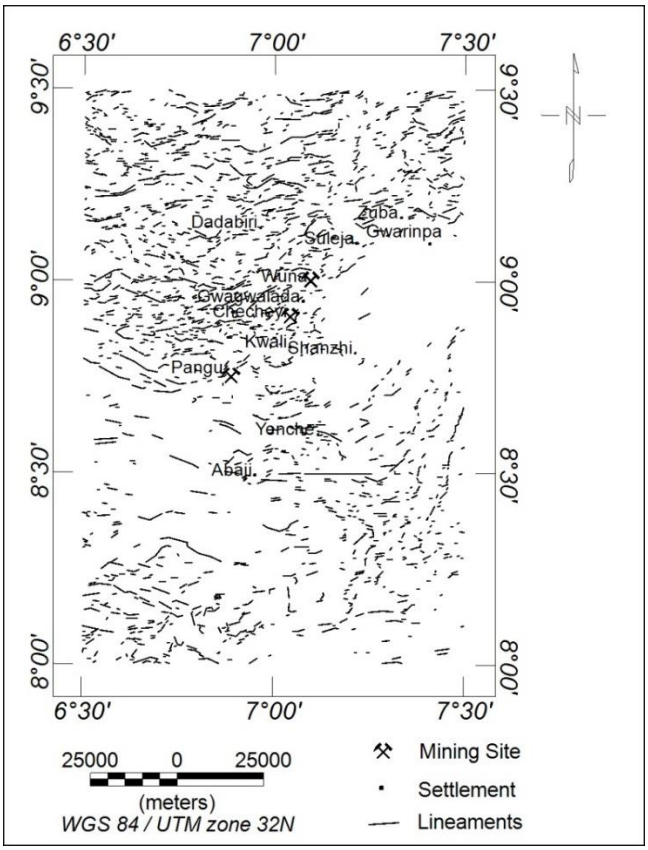

Fig. 7a. Lineament map derived from CET grid analysis depicting faults

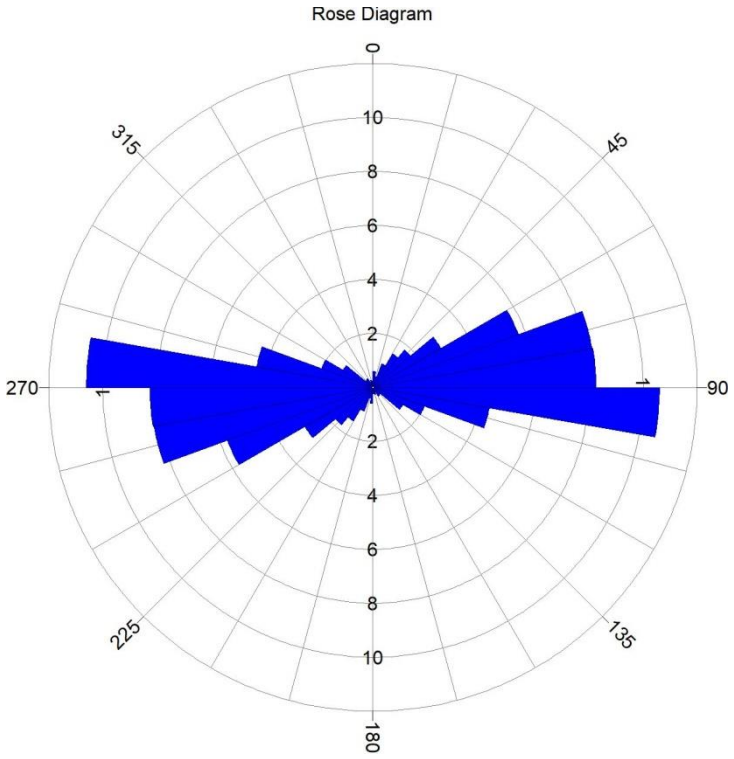

Fig. 7b. Rose diagram showing the structural trending direction of the study area

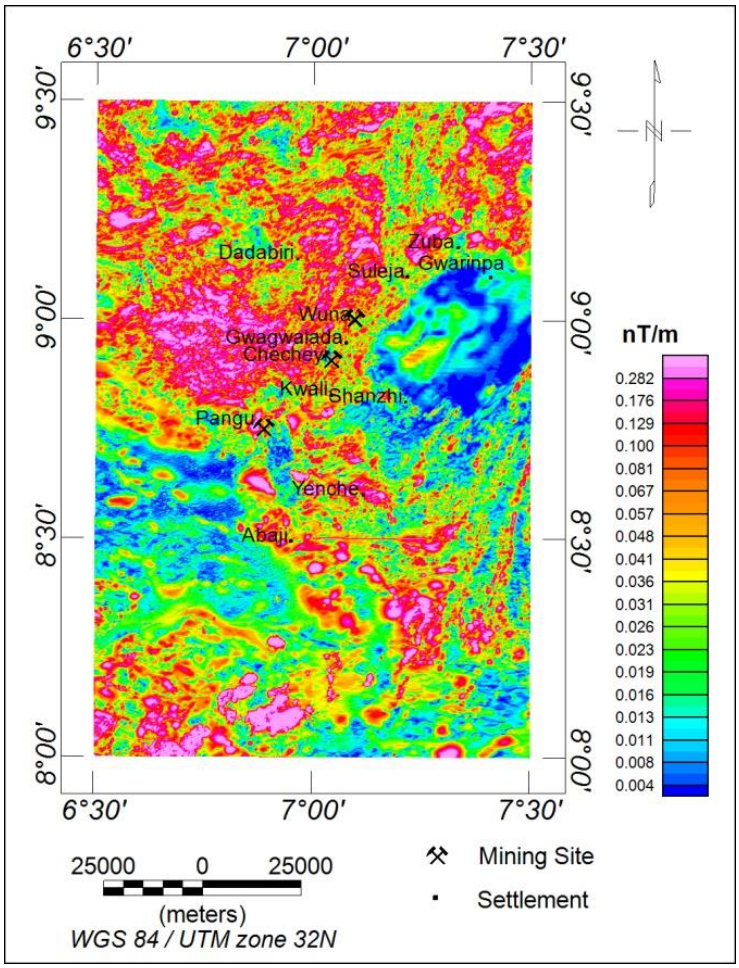

Fig. 8. Analyic Signal map of the study area

The Analytic Signal interpretation method was used to detect the boundaries and connections of the magnetic source bodies, as shown in Fig. 8.

These were identified as magnetic highs or lows in specific locations within the study area. The areas with very high frequency amplitudes of the analytic signal correspond with very high concentration of lineaments. The analytic signal map exhibits two to three different magnetic zones, the very high, the moderate and the low magnetic zones. The zones of high magnetic anomalies in the northern part are related to migmatite, gneisses, and biotite while the high magnetic anomalies correspond with sandstone, siltstone and shale (Fig. 3). The central region with moderate magnetic intensity is associated with schist rock formations. The areas around latitude N 8′30″ latitude N 9′00″ with lower magnetic intensity are associated with loose, unconsolidated sedimentary deposits. The zones with lower magnetic field amplitudes are likely indicative of suspected hydrothermal alteration having taken place in those areas. This is because hydrothermal alteration occurs when hot fluids interact with and change the mineralogical composition of the surrounding rock. This type of alteration can reduce the magnetic properties of the affected rock, leading to lower amplitude magnetic signatures in those regions.

The Euler deconvolution technique by Nabighian [39] found application in determining the depth to the magnetic basement through the utilization of the Euler equation on the RTP magnetic data. Tawey et al. [43] also used the Euler Deconvolution method to delineate the depth and location of the basement rock contact and/or faults with dykes. According to the Euler deconvolution analysis, the result suggests that the magnetic sources in the region span a wide range of depths. Specifically, the depth estimates indicate the following: sources deeper than 2000 meters, sources between 1000 and

2000 meters, sources between 500 and 1000 meters and sources shallower than 500 meters. The results further show that most of the highly magnetic structures and intrusive depth sources are located at depths between less than 100 meters and 500 meters, as illustrated in Fig. 9. When the results of the Euler deconvolution analysis are compared to the analytic signal map, first vertical derivative map and lineament map, it can be observed that the areas with high magnetic intensity, high frequency magnetic response, and high lineament concentration respectively conformed with a relatively shallow depth range, generally less than 100 to 500 meters which also with the location of local mining sites within the study area.

4.2 Aeroradiometric Data Interpretation

Four maps were utilized to analyze the aero-radiometric data. One map represented the potassium (K (%)) levels, another depicted the thorium (eTh (ppm)) values, a third map showed the uranium (eU (ppm)) concentrations, and the fourth map displayed the ratio of potassium to thorium (K/Th).

It can be seen in Fig. 10 that the K map shows elevated potassium concentrations. Pink colour is associated with very high K values (20.392-26.824%) which depicts the granitic and migmatitic rocks. The blue colour (5.841-10.220%) is associated with low K levels and this depicts claystones, sandstones and pebbles. Shades of orange to yellow indicate or are connected to relatively low K values, whereas red denotes moderately high to high K levels. These pinkish colorations, which are indicative of extremely high K values, are seen in the vicinity of Suleja, Zuba,Gwarinpai, Wuna, and Gwagwalda (which is north-central part of the study area). The regions immediately to the south of Kwali (Checheyi) and Yenche in the central portion of the map also show high concentration of K.

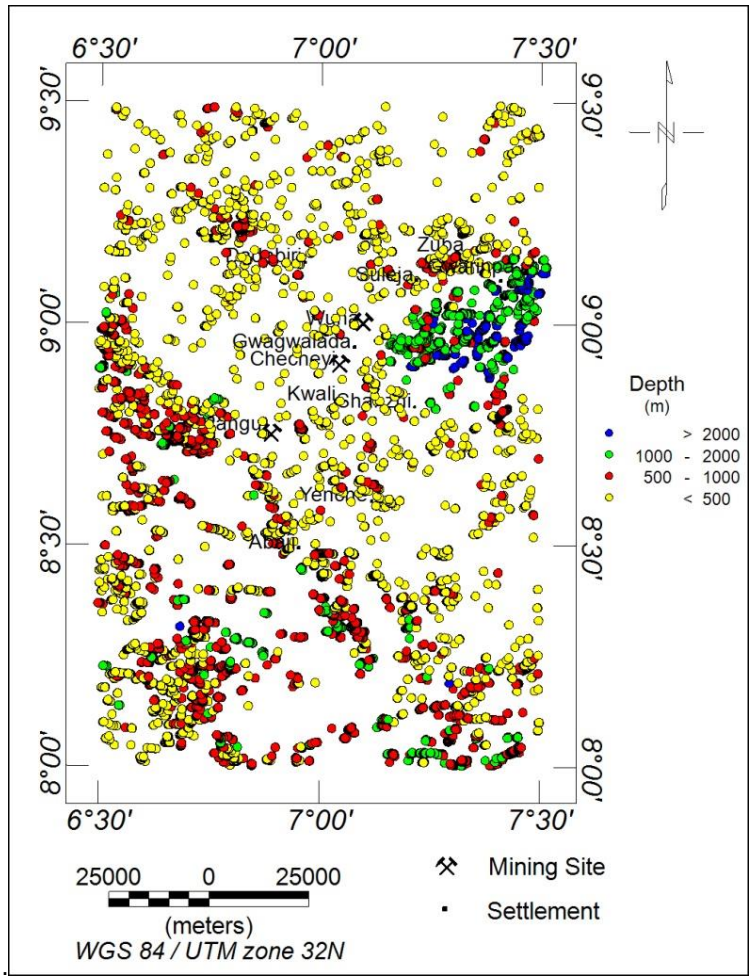

Fig. 9. 3-D Euler depth solution

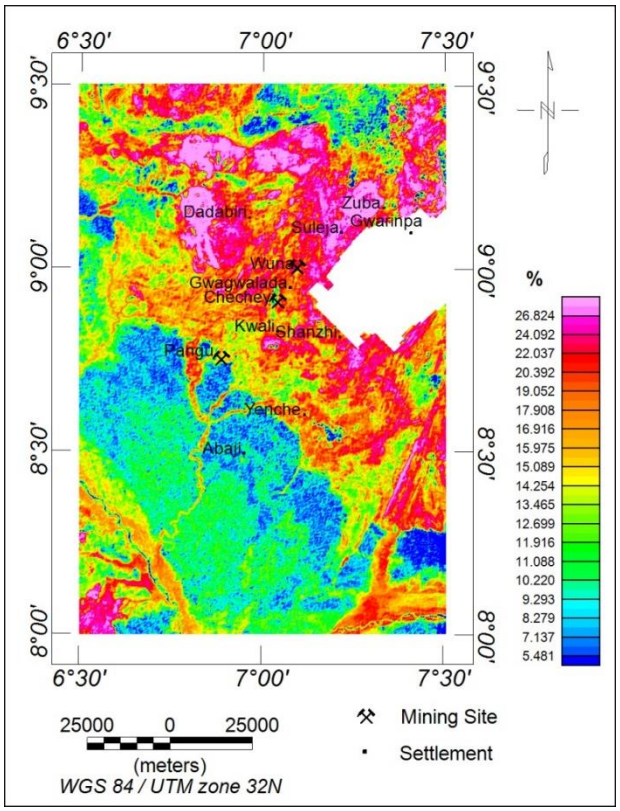

Fig. 10. Potassium concentration map

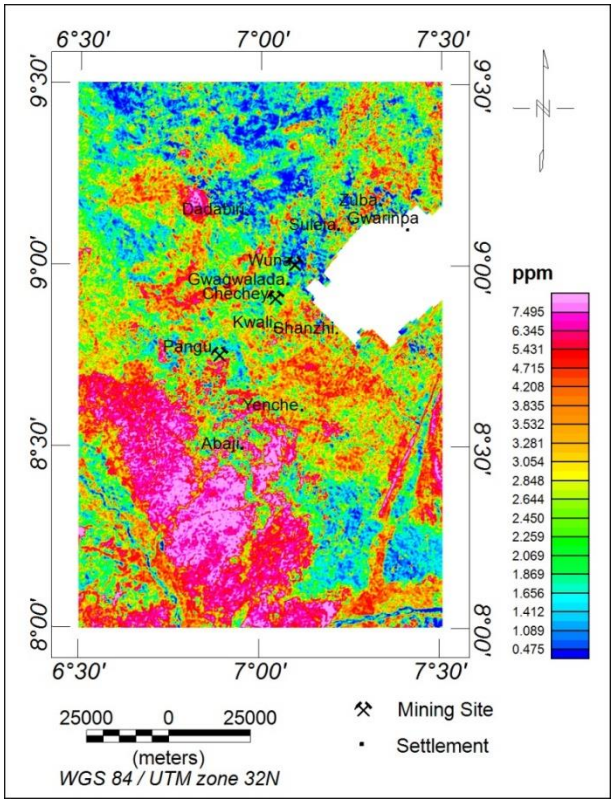

Fig. 11. Equivalent Uranium concentration map

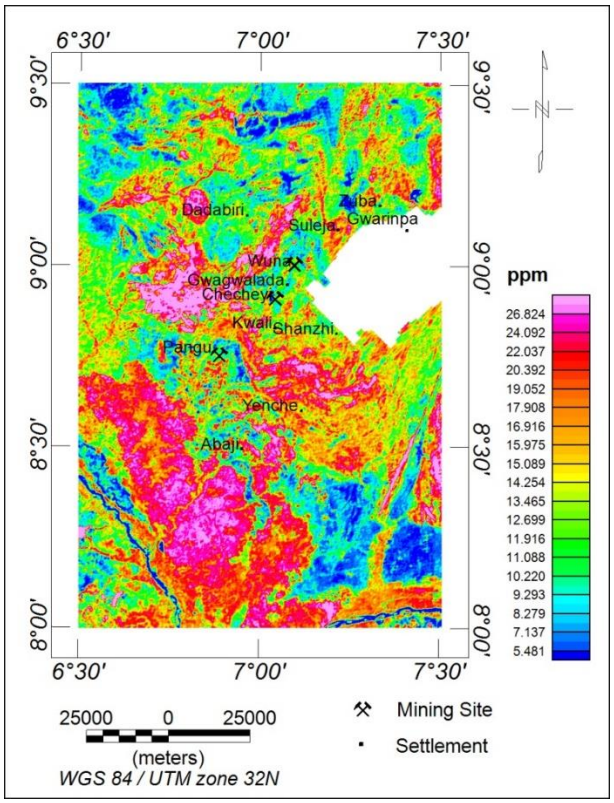

Fig. 12. Equivalent Thorium (eTh) concentration map

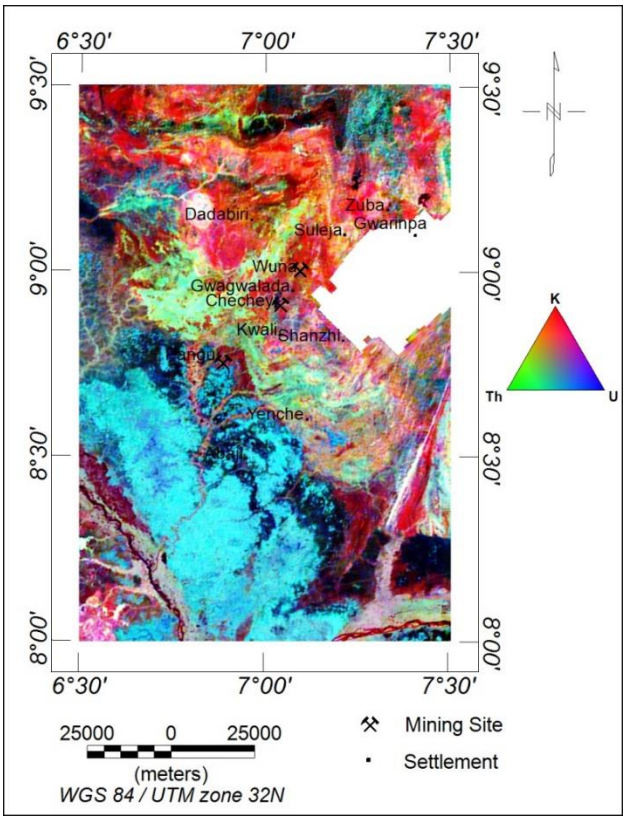

Fig. 13. Ternary image of the study area

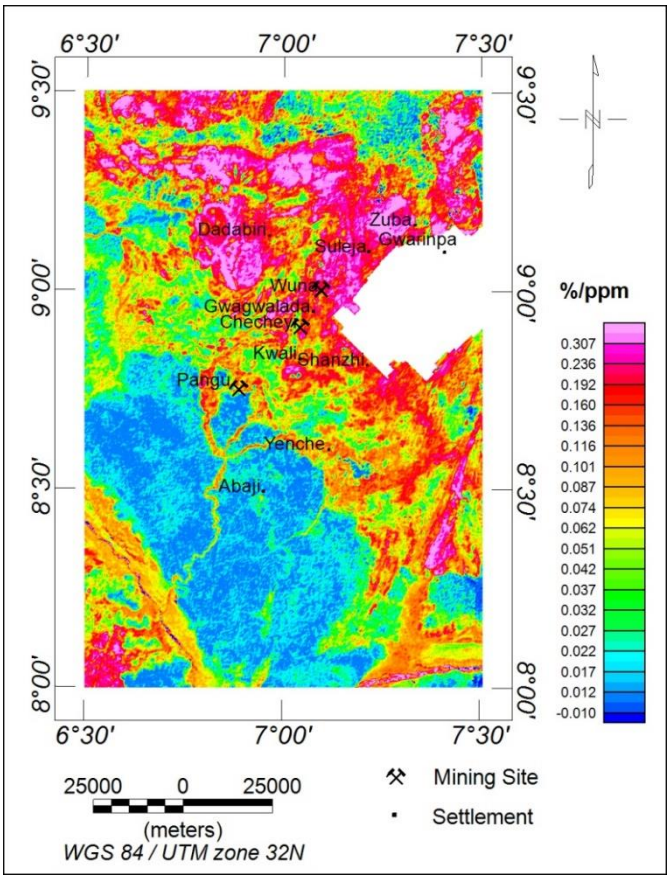

Fig. 14. Potassium/Thorium ratio map of the study area

The equivalent uranium (eU) map (Fig. 11) shows that porphyritic granite, biotite granite, granite gneiss, and migmatite rocks are related with high concentration values (6.345-7.495ppm) whereas clay, sandstones, pebbles, and grits are linked to low concentration (0.475-1.869ppm).

The equivalent thorium (eTh) map (Fig. 12) exhibits signatures similar to those of the uranium concentration map, which implies a similar lithological classification. However, the high-level concentration of thorium is delineated to be in the range of 20.392-26.824 ppm, while the low concentration is in the range of 5.841-10.220ppm.

The relative abundances of the three major radioactive elements; uranium (eU), thorium (eTh), and potassium (K)—within the research area are shown in the radioelement ternary map (Fig. 13). The activity concentrations of K, eTh, and eU were modulated to produce red, green, and blue colours, respectively, to make this ternary map. The sparse patches of bright color in the ternary image indicate areas where the concentrations of potassium (K), thorium (eTh), and uranium (eU) are elevated. This is likely due to the presence of granitic outcrops or sediments that have been derived from granite rocks in those locations. The regions with low concentrations of potassium (K), thorium (eTh), and uranium (eU) are highlighted in black on the map. This low radioelement signature may be indicative of the presence of mafic and ultramafic schist rock types in those areas.

Signals associated with zones of hydrothermal alteration can be identified quite effectively by using the K/Th ratio map. Ore deposits often exhibit hydrothermal alteration, which is characterized by an increase in the relative concentration of potassium (K) and a decrease in the relative concentration of thorium (Th). This relationship is depicted graphically in the K/Th map, as shown in Fig. 14. The high K/Th ratio map values indicate potential mineral deposits [44,45]. This study's K/Th ratio map indicates a range of values from 0.010 to 0.307 %/ppm. K/Th ratio of more than 0.192%/ppm, which corresponds to the pink coloration, is thought to represent the hydrothermally altered zones (Fig. 14). Hydrothermal alteration zones are

associated with structural relationships, suggesting that these structures functioned as pathways for the passage of hydrothermal fluids that simultaneously interacted with rock formations to produce alteration. The regions displaying hydrothermal alteration correspond with the lineaments presented in Fig. 7a, which suggest zones of mineralization. The presence of lineaments within these alteration zones strongly suggests that gold mineralization has the potential to occur in the area [46].

5. CONCLUSION

The utilization of aeromagnetic and aero-radiometric data facilitated the identification of geological features and prospective sites for gold exploration. Based on the study's findings, the area appears to be highly fragmented, with fractures trending northwest-southeast acting as conduits for hydrothermal fluids. These fluids have altered the surrounding rock formations, making them potential targets for the exploration of concealed gold. The analytic signal map reveals three magnetic zones: very high, moderate, and low, with high anomalies in northern parts attributed to migmatite, gneisses, and biotite. The Euler deconvolution technique, developed by Nabighian [39], is used to determine the depth to magnetic basements using RTP magnetic data. Tawey et al. [43] also use this method to identify basement rock contact and faults with dykes. The analysis shows that magnetic sources in the region have a wide range of depths, with most highly magnetic structures and intrusive depth sources located between 100 and 500 meters. The tilt derivative map helped in delineation of horizontal location and extent of edges of various causative sources while the first vertical derivative map aided in structural delineation within the study area. Signals associated with zones of hydrothermal alteration can be identified quite effectively by using the K/Th ratio map. Ore deposits often exhibit hydrothermal alteration, which is characterized by an increase in the relative concentration of potassium (K) and a decrease in the relative concentration of thorium (Th). This relationship is depicted graphically in the K/Th map, as shown in Fig. 14. The high K/Th ratio map values indicate potential mineral deposits [44]. This study's K/Th ratio map indicates a range of values from 0.010 to 0.307 %/ppm. K/Th ratio of more than 0.192%/ppm, which corresponds to the pink coloration, is thought to represent the hydrothermally altered zones (Fig. 14). Hydrothermal alteration zones are associated with structural relationships, suggesting that these structures functioned as pathways for the passage of hydrothermal fluids that simultaneously interacted with rock formations to produce alteration. The regions displaying hydrothermal alteration correspond with the lineaments presented in Fig. 7a, which suggest zones of mineralization. The presence of lineaments within these alteration zones strongly suggests that gold mineralization has the potential to occur in the area deposits.

DISCLAIMER (ARTIFICIAL INTELLIGENCE)

Author(s) hereby declare that NO generative AI technologies such as Large Language Models (ChatGPT, COPILOT, etc) and text-to-image generators have been used during writing or editing of manuscripts.

ACKNOWLEDGEMENT

The paper is part of Ph. D thesis of Bwamba J.A. The authors sincerely appreciate the Nigeria Geological Survey Agency (NGSA) for releasing the data used for the study. Our appreciation also goes to the management of the Sheda Science and Technology Complex (SHESTCO) for their moral support.

COMPETING INTERESTS

Authors have declared that no competing interests exist.

REFERENCES

1. Abdelrahman EM, Soliman KS, El-Araby TM, Abo-Ezz ER and Essa KS A least-squares standard deviation method to interpret magnetic anomalies due to thin dikes. Near Sur Geophys. 2009;7:41–46.
2. Akbar S, Fathianpour N. Improving the curie depth estimation through optimizing the spectral block dimensions of the aeromagnetic data in the Sabalan geothermal feld. J Appl Geophy. 2016;135:281–287.
3. Le Maire P, Munschy M. 2D Potential feld theory using complex algebra: New equations and vizualisation for the interpretation of potential feld data. Geophysics. 2018;83:J1–J13.
4. Arinze IJ, Emedo CO. Integrated geophysical investigation for shallow-scale

massive (Pb-Zn) sulphide and barite exploration in the abakaliki and obubra mining districts (AOMD), Southeastern Nigeria. Min Metall Explor. 2021;38:381–395.

5. Bwamba, Jonah Ayuba, Abu Mallam and Abel U. Osagie. Characterization of hydrothermal alteration zones in parts of north-central basement complex of Nigeria for Solid Mineral Deposits. Earth Sciences Pakistan. 2024;8(2):72-79.
6. El - Sadek MA. Application of thorium-normalized airborne radio-spectrometric survey data of Wadi Araba area, North-eastern Desert, Egypt, as a guide to the recognition of probable subsurface petroleum accumulations. Applied Radiation and Isotopes, U.S.A. 2002;57:121 – 130.
7. Mehanee S, Essa KS, Diab ZE. Magnetic data interpretation using a new r-parameter imaging method with application to mineral exploration. Nat Resour Res. 2021;30:77–95.
8. Goldfarb RJ, Groves DI. Orogenic gold: Common or evolving fl uid and metal sources through time," Lithos. 2015;233:2–26.
   DOI: 10.1016/j.lithos.2015.07.011
9. Saibi H, Azizi M, Mogren S. Structural investigations of afghanistan deduced from remote sensing and potential field data, Acta Geophysica. 2016;64(4):978–1003.
   DOI: 10.1515/acgeo-2016-0046
10. Saadi NM, Aboud E, Saibi H, Watanabe K. Integrating data from remote sensing, geology and gravity for geological investigation in the tarhunah area, Northwest libya, Int J Digit Earth. 2008;1(4):347–366.
    DOI: 10.1080/17538940802435844
11. Bersi M, Saibi H, Chabou MC. Aerogravity and remote sensing observations of an iron deposit in Gara Djebilet, southwestern Algeria, Journal of African Earth Sciences. 2016;116:134–150.
    DOI: 10.1016/j.jafrearsci.2016.01.004
12. Azizi M, Saibi H, Cooper GRJ. Mineral and structural mapping of the Aynak-Logar Valley (eastern Afghanistan) from hyperspectral remote sensing data and aeromagnetic data, Arabian Journal of Geosciences 2015 8:12:10911–10918.
    DOI: 10.1007/S12517-015-1993-2
13. Pendry JB, Holden AJ, Robbins DJ, Stewart WJ. Magnetism from conductors and enhanced nonlinear phenomena, IEEE Trans Microw Theory Tech. 1999;47(11):2075–2084.
    DOI: 10.1109/22.798002
14. Olomo KO, Bayode S, Alagbe OA, Olayanju GM, Olaleye OK. Aeromagnetic mapping and radioelement influence on mineralogical composition of mesothermal gold deposit in part of ilesha schist belt, Southwestern Nigeria, NRIAG Journal of Astronomy and Geophysics. Dec. 2022;11(1):177–192.
    DOI: 10.1080/20909977.2022.2057147
15. Schetselaar EM, Harris JR, Lynds T, De Kemp EA. Remote predictive mapping (RPM): A strategy for geological mapping of canada north, Journal of geoscience, Canada. 2007;34:93–111.
16. Komolafe AA, Kuria ZN, Woldai T, Noomen M, Yekini A, Anifowose B. Integrated remote sensing and geophysical investigations of the geodynamic activities at lake magadi, Southern Kenyan Rift. 2012;2012.
    DOI: 10.1155/2012/318301
17. Palomera AD. Application of remote sensing and geographic information systems for mineral predictive mapping, Deseado Massif, Southern Argentina by, University of Twente, ITC Thesis; 2004.
18. El- Sadek MA, Ammar AA, Sabry AM. Aeroradiospectro- metry in the lithological mapping and environmental monitoring of Wadi Araba area. The Arabian Journal for Science and Engineering. 2002;27(2A):131 –148.
19. Behnia P, Harris JR, Rainbird RH. Williamson MC, Sheshpari M. Remote predictive mapping of bedrock geology using image classification of Landsat and SPOT data, western Minto Inlier, Victoria Island, Northwest Territories, Canada," Int J Remote Sens. Nov. 2012;33(21):6876–6903.
    DOI: 10.1080/01431161.2012.693219
20. Dickson BL, Scott KM. Interpretation of aerial gammaray surveys-adding the geochemical factors, Journal of Australian Geology and Geophysics. 1997;17(2): 187–200.
21. Sayed E, Selim I. The use of magnetic and geo-electrical data to delineate the subsurface structures and groundwater potentiality in Southeastern Sinai, Egypt, Springer, 2013;1479– 1494.
    DOI: 10.1007/s12665-013-2234-1

22. Keating P, Pilkington M. Euler deconvolution of the analytic signal and its application to magnetic interpretation. 2004;165–182.
23. Boszczuk P, Zhen L, Roy P, Lacroix S, Cheilletz A. A 3D gravity data interpretation of the Matagami mining camp, Abitibi Subprovince, Superior Province, Québec, Canada Application to VMS deposit exploration. 2011;75:77–86.
DOI: 10.1016/j.jappgeo.2011.06.031
24. Gaafar IM. Geophysical signature of the vien-type uranium mineralization of Wadi Eishimbai, Southern Eastern Desert. 2012;1185–1197.
DOI: 10.1007/s12517-010-0263-6
25. El-Sadek MA. Radiospectrometric and magnetic signatures of a gold mine in Egypt. Journal of Applied Geophysics. Netherlands, Elsevier B. V. 2009;67:34 - 43.
26. Wang J. et al., Lithologic mapping test for gravity and magnetic anomalies A case study of gravity – magnetic anomaly pro fi le in the eastern segment of the China – Mongolia border, J Appl Geophy. 2015;117:23–31.
DOI: 10.1016/j.jappgeo.2015.03.020
27. Aliyu SB, Adetona AA, Rafiu AA, Ejepu J, Adewumi T. Delineating and Interpreting the gold veins within Bida and Zungeru Area, Niger State Nigeria, Using Aeromagnetic and Radiometric Data. Pakistan Journal of Geology. 2021;5(2):41-50.
DOI: 10.2478/pjg-2021- 0006
28. Imasuen OI, Olatunji JA, Ibitoye VT. Geological observations of basement rocks, around Ganaja, Kogi state, Nigeria. Jour. Sci. Multidiscip. Res. 2010;2:87-102.
29. Amigun JO, Afolabi O, Ako BD. Euler 3-D deconvolution of analytical signal of magnetic anomalies over iron ore deposit in Okene, Nigeria. Jour. Emerging Trends Engg. Appld. Sci. (JETEAS). 2012;3(4):711-717
30. Anudu GK, Onuba LN, Onwuemesi AG, Ikpokonte AE. Analysis of aeromagnetic data over Wamba and its adjoining areas in North Central Nigeria. Earth Sci. Res. Jour., v. 2012;16(1):25-33.
31. Abbass AA, Mallam A. Estimating the thickness of sedimentation within lower benue basin and upper Anambra Basin, Nigeria, using both Spectral Depth Determination and Source Parameter Imaging. Geophysics; 2013.
32. Daniel E, Jimoh R, Lawal K. Delineation of gold mineral potential zone using high resolution aeromagnetic data over part of Kano State, Nigeria. Journal of Geology and Geophysics. 2019;8:464.
DOI: 10.35248/2381-8719.464
33. Ayuba RA, Nur A. Analysis of high resolution aeromagnetic data and satellite imagery for mineral potential over parts of Nasarawa and environs. North-Central Nigeria. International Journal of Scientific and Technology Research. 2018;7(6).
34. Jamaluddeen SS, Aku MO, Saleh M, Bunawa AA, Sharafa SB. A reconnaisance study to delineate the potential mineral zones around the schist belt areas of Kano State, Nigeria using airborne magnetic data. Journal of Geology and Mining Research. 2018;11(2):14-21.
35. Rahaman MA. Recent advances in the study of the basement complex of Nigeria. In Precambrian Geol. Niger. In Bull. 1988;32:11-43.
36. Obaje NG. The basement complex. In: Geology and Mineral Resources of Nigeria. Lecture Notes in Earth Sciences, vol 120. Springer, Berlin, Heidelberg; 2009.
Available:https://doi.org/10.1007/978-3-540- 92685-6_2
37. Geosoft, Oasis montaj Viewer 7.0 The core software platform for working with large volume spatial data Quick Starttm Tutorial; 2008.
38. Milligan PR, Gunn PJ. Enhancement and presentation of airborne geophysical data, AGSO J. Geol. Geophys. 1997;17(2):63–75.
39. Nabighian MN. The analytic signal of two-dimensional magnetic bodies with polygonal cross- section: Its properties and use for automated anomaly interpretation, Geophysics. 1972;37(3): 507–517.
40. Verduzo B, Fairhead JD, Green CM, MacKenzie C, New insights into magnetic derivatives for structural mapping: The Leading Edge, v. 2004;23:116-119.
41. Nabighian MN, Hansen RO. Unification of euler and werner deconvolution in three dimensions via the generalized hilbert transform. Geophysics. 2001;66:1805-1810.
42. Shives RBK, Charbonneau BW, Ford KL. The detection of potassic alteration by gamma ray spectrometry - recognition of

alteration related to mineralization, Radiation Geophysics. 1997;416:1–17.

43. Tawey MD, Alhassan DU, Adetona AA, Salako KA, Rafiu AA, Udensi EE. Application of aeromagnetic data to assess the structures and solid mineral potentials in part of north central Nigeria. Journal of Geography, Environment and Earth Science International. 2020;24(5):11-29. 2020; Article no Journal of Geography, Environment and Earth Science International 24(5):11-29, 2020; Article no.JGEESI.58030 ISSN: 2454-7352. JGEESI.58030 ISSN: 2454-7352
44. Akinlalu AA. Radiometric mapping for the identifcation of hydrothermally altered zones related to gold mineralization in IfeIlesa Schist Belt, Southwestern Nigeria. Indones. J. Earth Sci. 2023;3:A519–A519.
45. El-Sadek MA Using of airborne gamma-ray spectrometric data to the exposure of potassic alteration -recognition of alteration relates to gold mineralization. Applied Radiation and Isotopes. 2022; 190:110511.
46. Salako KA. Depth to basement determination using source parameter imaging (SPI) of aeromagnetic data: An application to upper Benue Trough and Borno Basin, North East Nigeria. Academic Res. Internat., v. 2014;5(3):74-86.

Peer-review history:
The peer review history for this paper can be accessed here:
https://www.sdiarticle5.com/review-history/119595